PEMBROKE INSTRUMENTS, LLC
pembrokeinstruments.com | sales@pembrokeinstruments.com | +1-650-550-8618

International Journal of Pharmaceutics 702 (2026) 127174

Contents lists available at ScienceDirect

International Journal of Pharmaceutics

journal homepage: www.elsevier.com/locate/ijpharm

Direct comparison of near-infrared spectroscopy with near-infrared spatially resolved spectroscopy for monitoring active pharmaceutical ingredient concentration in a feed frame simulator

Eleonora De Giorgi [a,b,*], Sean Clifford [b], Kevin Sutcliffe [b], Nathan Cumberbatch [b], Estefania Lopez-Quiroga [a], Christopher Windows-Yule [a]

[a] School of Chemical Engineering, University of Birmingham, Edgbaston, B15 2TT, UK
[b] Global Product Development, Pharmaceutical Technology & Development, Operations, AstraZeneca, Macclesfield, UK

ARTICLE INFO

Keywords:
Near-infrared spectroscopy
Process Analytical Technology
Continuous Direct Compression
Manufacturing
Feed frame simulator
Modelling

ABSTRACT

As pharmaceutical manufacturing shifts towards continuous processing and increasingly potent, low-dose Active Pharmaceutical Ingredient (API) products, there is a growing need for more accurate and reliable Process Analytical Technology (PAT). This study presents a direct, side-by-side comparison of Near-Infrared (NIR) spectroscopy and Near-Infrared Spatially Resolved Spectroscopy (NIR-SRS) for API concentration monitoring within a Continuous Direct Compression (CDC) process, using a Feed Frame Simulator (FFSIM). Both probes simultaneously measured moving powder under dynamic conditions to assess their modelling performance. Instrument settings, including the number of spectral averages, were selected to ensure the consistent measurement of a unit-dose for both instruments. The resulting datasets were processed and Partial Least Squares (PLS) models were built. Root Mean Square Error (RMSE) values indicate that NIR-SRS performed comparably to NIR, resulting in similar error values and marginally higher concentration detection limits; however, its narrower wavelength range currently limits its suitability for drug loading quantification and modelling, particularly for low-dose formulations where broader spectral coverage is critical to enhance model robustness and sensitivity.

1. Introduction

Pharmaceutical manufacturing for drug substance and drug product has undergone a significant shift over the last two decades from traditional batch manufacturing to continuous processing. This enables much faster production, fewer process steps, and more consistent product quality, as well as easier scale-up and greater equipment flexibility (De Leersnyder et al., 2019). For drug product, a large portion of the market focuses on oral solid dosage forms, with Continuous Direct Compression (CDC) emerging as the leading production method (Román-Ospino et al., 2021). By avoiding the wet granulation phase and directly compressing dry raw materials, the need for a solvent and drying step is removed, leading to significant time and resource savings and improved sustainability.

Monitoring powder formulation quality during the CDC tableting process to maintain product specifications is complex. Critical Quality Attributes (CQAs), including Active Pharmaceutical Ingredient (API) quantification and blend uniformity, are controlled by adjusting Critical Process Parameters (CPPs) as a key component of the overall control strategy. Determining appropriate CPP changes solely from process data, such as powder flow rates and compression forces, as well as off-line product analysis is challenging; however, this can be significantly improved by employing an enhanced control strategy that incorporates chemometric modelling through Process Analytical Technology (PAT) (Rosas et al., 2023). The Food and Drug Administration (FDA) outlined a guidance in 2004 which details the appropriate application of PAT and encourages industry to employ it as a non-destructive analysis technique to design and understand processes while enhancing process control (FDA, 2004). PAT sensors allow in-line CQA and process monitoring, reducing the time and effort required for both sampling and off-line analysis, as well as their associated risks (Román-Ospino et al., 2021). Of the various available techniques, Near-Infrared (NIR) spectroscopy is the most utilised in the pharmaceutical industry for various applications, from blending (Bouckaert et al., 2025) to granulation (Palmer et al., 2020) and tabletting (Peeters et al., 2023; Ryckaert et al., 2025). This is mostly due to its applicability across a range of solids, its safety compared to laser-based systems as it utilises a

* Corresponding author at: School of Chemical Engineering, University of Birmingham, Edgbaston, B15 2TT, UK.
E-mail address: eleonora.degiorgi@astrazeneca.com (E. De Giorgi).

https://doi.org/10.1016/j.ijpharm.2026.127174
Received 10 April 2026; Received in revised form 30 June 2026; Accepted 9 July 2026
Available online 22 July 2026
0378-5173/© 2026 The Authors. Published by Elsevier B.V. This is an open access article under the CC BY license (http://creativecommons.org/licenses/by/4.0/).

PEMBROKE INSTRUMENTS
pembrokeinstruments.com | sales@pembrokeinstruments.com | +1-650-550-8618

PEMBROKE INSTRUMENTS, LLC
pembrokeinstruments.com | sales@pembrokeinstruments.com | +1-650-550-8618

lamp as the light source, low costs of implementation and maintenance, high robustness and small scale, which makes it simple to integrate in-line for various processes (Bhimrao et al., 2026). Being a rapid, non-destructive and non-invasive technology, its uses include monitoring of blend content uniformity, mixing endpoint determination and API level quantification (Rangel-Gil et al., 2024; De Leersnyder et al., 2018). This study will focus on technology application within the feed frame of a tablet press, which is a chamber collecting the blended formulation from a hopper and uniformly distributing it into the die cavities for compression into tablets of equal weight and composition, with the aid of rotating paddles. This has been selected as it is the last stage prior to tablet compression where a model could be used to make a quality decision on the formulation in real time, enabling a divert to waste strategy if the product is out of specification (Sierra-Vega et al., 2019; Román-Ospino et al., 2021; Ortega-Zúñiga et al., 2025; Ryckaert et al., 2025). It is also the most representative stage to measure API content other than the standard chromatographic methods performed on ejected tablets, as it is the closest measurement point to the die cavities where the blend is turned into the final product (Li et al., 2019).

The currently widely used NIR spectroscopy is not sufficiently performant in some cases and faces challenges when approaching the quantitation limit (the lowest quantity of a substance that can be reliably measured), such as with low dose API formulations or compounds of interest that are not as responsive to it (Brouckaert et al., 2022; Román-Ospino et al., 2021; FDA, 2018). Therefore there is a need to identify and compare alternative PAT solutions. NIR Spatially Resolved Spectroscopy (NIR-SRS) utilises multiple fibres, offering an advantage over a single collection fibre, as it can sample mass at multiple points for an improved spatial representation of the blend contents and their homogeneity (Igne et al., 2015). In the configuration investigated, the benefit of NIR-SRS can be described as improved averaging across local heterogeneity rather than direct resolution of individual particles. Given that effective measurement for both techniques was at a broader, millimetre-scale sampled region, the analytical response reflected a spatially averaged powder volume. Via the use of light scattering phenomena which allow the light to be absorbed further into the sample before being collected by the fibres, more information is acquired to improve the determination accuracy of the sample API concentration, thus increasing instrument sensitivity (Brouckaert et al., 2022). The fibres can also be placed at various distances away from the illumination source, covering different penetration depths into the sample (Román-Ospino et al., 2021). Being less complex than hyperspectral chemical imaging, NIR-SRS is able to acquire large volumes of data at a pace that is suitable for in-line analysis of formulations and tablets (De Man et al., 2023).

Testing NIR-SRS on a large scale tablet press is time and material intensive, while requiring the expertise of operators to run the press. This would generate significant material wastage due to upstream and press system adjustments leading to extended time periods to reach steady state and the continuous ejection of out-of-specification material into the waste stream. Therefore this study is performed in a Feed Frame Simulator (FFSIM), a chamber with a rotating paddle wheel which closely replicates the environment within a tablet press feed frame. The FFSIM was not intended to demonstrate complete equivalence to a commercial tablet press in every operational aspect, but rather to reproduce the key conditions governing powder–probe interactions immediately prior to compression. As such, it provided a suitable platform for a controlled head-to-head technology comparison under matched dynamic conditions. It has the possibility to run in recirculation mode by closing the outlet port, only requiring approximately 200 g of powder per run rather than kilograms (Colaço Botelho Mestre, 2023; Expo Process Analytics, 0000). It is simple to operate and offers the opportunity to test two probes simultaneously, hence this study is comparing single point measurement NIR with NIR-SRS in a side-by-side investigation. The methodology developed by the author is a first application of NIR-SRS with the FFSIM as well as a direct comparison of both technologies together, showing that these in-line instruments can be successfully integrated into development platforms as well as tablet presses and result in successful data collection and model building.

While the authors acknowledge that the formulations used range from low to high dose in a single model, the findings are still applicable to building a framework to test low dose formulations in isolation. The main aspects covered include sensor data collection capabilities, speed of acquisition, Partial Least Squares (PLS) model building and the ability to develop models at small scale for future transfer to larger scale processes. This remains at the forefront of the ongoing efforts to develop robust real-time release testing strategies for an extensive range of products, using validated in-process measurements and models to assure quality and support release without relying solely on end-product testing.

Table 1
Contents of the excipient and Product A formulations tested.

Excipient formulation components (% w/w)	
Lactose	MCC
0.5	99.5
1.5	98.5
3.0	97.0
10.0	90.0
20.0	80.0
30.0	70.0

Product A formulation components (% w/w)			
Product A	Mannitol	MCC	Croscarmellose sodium
0.5	70.3	25.2	4.0
1.5	69.3	25.2	4.0
3.0	67.8	25.2	4.0
10.0	60.8	25.2	4.0
20.0	50.8	25.2	4.0
30.0	40.8	25.2	4.0

2. Materials and methods

2.1. Materials

Model excipient formulations as well as Product A formulations were used in this study. The excipient blends consisted of lactose (Pharmatose 110 M, DFE Pharma, Goch, Germany) as the surrogate API and Microcrystalline Cellulose (MCC) (Avicel® PH-102, FMC biopolymer, Cork, Ireland). Lactose was selected to represent the API due to its similar physical properties to a range of APIs, its low toxicity and wide availability at low cost. The lactose concentration in the powder blends ranged between 0.5% w/w and 30% w/w, as listed in Table 1. The second set of Product A blends was utilised to demonstrate the application of this method on development formulations. These mixtures consisted of Product A as the API with mannitol (Pearlitol® 100 SD, Roquette, Lestrem, France), MCC (Vivapur 102, JRS Pharma, Rosenberg, Germany) and croscarmellose sodium (Ac-Di-Sol® SD-711, FMC Biopolymer, Philadelphia, United States) as the excipients. Similarly to the excipient blends, the concentration of Product A varied between 0.5% w/w and 30% w/w, as shown in Table 1.

The lactose and MCC components in the excipient formulation had approximate mean particle sizes of 130 μm and 100 μm respectively. In the Product A formulation the main excipient components, mannitol and MCC, had approximate mean particle sizes of 100 μm and 130 μm, whereas the API and croscarmellose sodium were finer, at approximately 41 μm and 24 μm. While these size differences may contribute to some local heterogeneity, substantial segregation during the study was not expected to be a dominant effect given the relatively similar size of the major excipient fractions and the short residence time of material in the feed frame simulator.

PEMBROKE INSTRUMENTS
pembrokeinstruments.com | sales@pembrokeinstruments.com | +1-650-550-8618

PEMBROKE INSTRUMENTS, LLC
pembrokeinstruments.com | sales@pembrokeinstruments.com | +1-650-550-8618

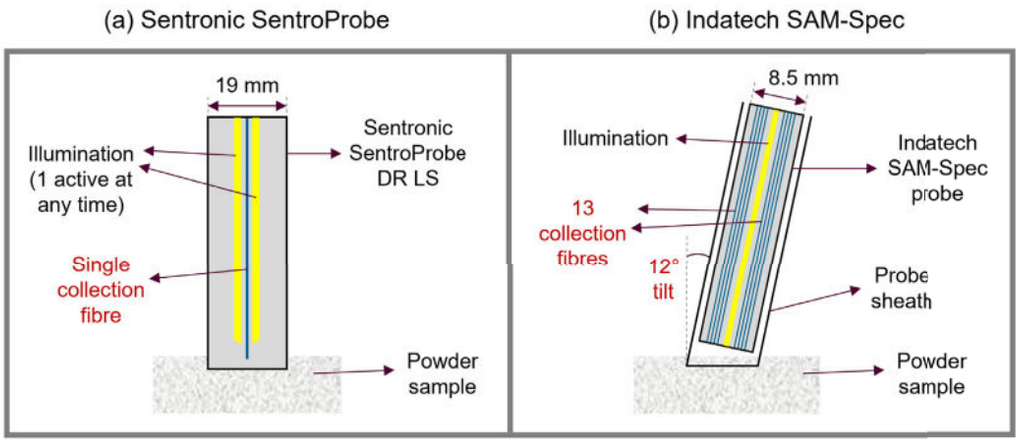


Fig. 1. Probe vertical cross-sections and configuration differences including the number of collection fibres and orientation with respect to the sample between (a) the Sentronic SentroProbe and (b) the Indatech SAM-Spec.

To ensure a fair comparison of the powder blends within the FFSIM such that the chamber fill level was maintained constant, these were manufactured at equivalent volumes of 1200 mL. Formulations were prepared by dispensing and screening the components through a 1 mm sieve into a 2500 mL Purovaso (ChargePoint, Campbell, USA) vessel and mixed using a Pharmatech MB015 uniaxial blender (Pharmatech, Coleshill, UK) for 24 min at 25 rpm. They were then separated equally by weight into 3 repeat blends and placed in 500 mL glass jars to be used with the feedframe simulator. The weights of each blend varied between 156 g and 172 g, according to the composition of each formulation.

2.2. Experimental design

All the blends were tested using the FFSIM from Expo Process Analytics (Cork, Ireland). These were inserted into the chamber gradually, in order to prime it and completely fill the available space. Any excess remained within the feed chute to ensure replication of typical tablet press conditions, with powder continuously filling the hopper above the feed frame. A constant paddle speed of 30 rpm was maintained for all experimental runs. This is within the operational range of commercial tablet presses and minimises shear stress on the powder blend given the extended residence time in the FFSIM compared to a continuous tablet press. The FFSIM paddle rotation was started when the chamber was completely full, and once the speed reached steady state the spectrometer measurements were started. This was repeated for all blends in increasing lactose or Product A concentration to minimise carry-over from higher-dose runs and avoid surrogate or API spikes between different runs due to chamber contamination. The equipment was cleaned by thorough vacuuming and the use of Isopropyl Alcohol (IPA) solvent between repeats.

2.3. NIR spectroscopy

The data were collected with two spectrometers simultaneously, the SentroPAT FO (Sentronic, Dresden, Germany) NIR system with the SentroProbe DR LS and the Hy-Ternity (Indatech, Clapiers, France) NIR-SRS system with the SAM-Spec probe, both in reflection mode and utilising diode array technology. The SentroProbe employs one illumination rod and a single fibre optic collection fibre, while the SAM-Spec has an illumination strip comprising a bundle of fibres, which are surrounded by 13 collection fibres as shown in Figs. 1 and 2. The data from the individual fibres is then either averaged into mean data or taken as separate spectra.

The SAM-Spec probe must be held at an angle of 12° from the perpendicular to the sample. This tilt reduces direct coupling of the illumination into the collection fibres, preventing detector saturation. By angling the probe, the incident light traverses a longer path through the sample, is attenuated, and then returns to the collection fibres with lower intensity. In contrast, the SentroProbe design addresses this inherently, as its illumination rods are cut at an angle within the probe shaft, directing light away from the collection fibre. Even with the probe held perpendicular to the powder bed, the collection fibre is therefore not flooded and saturation is avoided. The two instruments have different spectral ranges and resolutions. The SentroPAT FO detector works between 1100–2100 nm providing an absorbance value for each wavelength value, with a total of 1001 data points per spectrum, whereas the Hy-Ternity operates between 900–1650 nm with one data point every 3 wavelength values, resulting in 251 data points per spectrum.

2.3.1. Signal stability of the Sentronic SentroPAT FO and Indatech Hy-Ternity over time

A 4 h long static test was performed with both instruments, collecting spectra of a white reference standard and analysing the data with Principal Component Analysis (PCA). PCA can summarise high-dimensional, collinear NIR spectra into a few orthogonal Principal Components (PCs) to detect and visualise variability in the form of trends, drift and anomalies by separating systematic variation from noise. The test was used to detect any changes in the spectra of the same sample over time and determine the signal stability of the instrument. This was achieved by looking at the scores plot, which aids the visualisation of patterns such as clusters, drift and outliers between the samples within the PC space, as well as the loadings plot, to identify how each variable (wavelength) contributes to the PCs and overall variability. The Hotelling's T^2 metric is also used to quantify how far each sample score is from the model centre, flagging unusual or extreme observations within the modelled variation over time. For the Hy-Ternity system, data from individual fibres were also analysed to see if any presented more variability than others.

2.3.2. Dynamic data collection of NIR spectra in the FFSIM

The spectrometer probes were attached to the two measurement ports of the FFSIM and inserted into the chamber, in product contact, with a gap of 2 mm between the tip of the probe and the base of the paddle wheel notch (Fig. 3(b)). This ensured the probe tip was fully immersed in the moving powder at all times, while maintaining a sufficient distance from the paddle wheel to prevent any signal interference from the metal (De Leersnyder et al., 2018).

The SentroProbe has a shaft length of 170 mm and diameter of 19 mm, and it was inserted perpendicularly to the chamber into its adapter attached to the FFSIM, with a micrometer gauge to adjust its

PEMBROKE INSTRUMENTS
pembrokeinstruments.com | sales@pembrokeinstruments.com | +1-650-550-8618

PEMBROKE INSTRUMENTS, LLC
pembrokeinstruments.com | sales@pembrokeinstruments.com | +1-650-550-8618

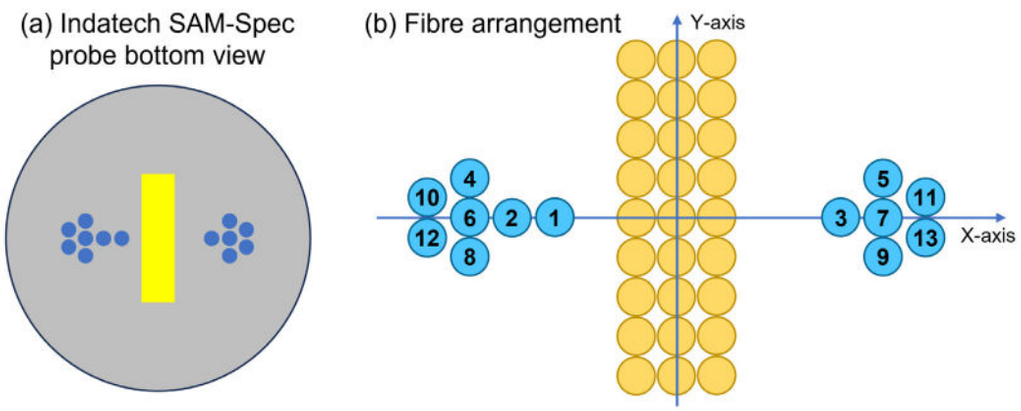


Fig. 2. SAM-Spec fibre configuration (a) bottom view (horizontal cross section) and (b) details of the fibre arrangement.

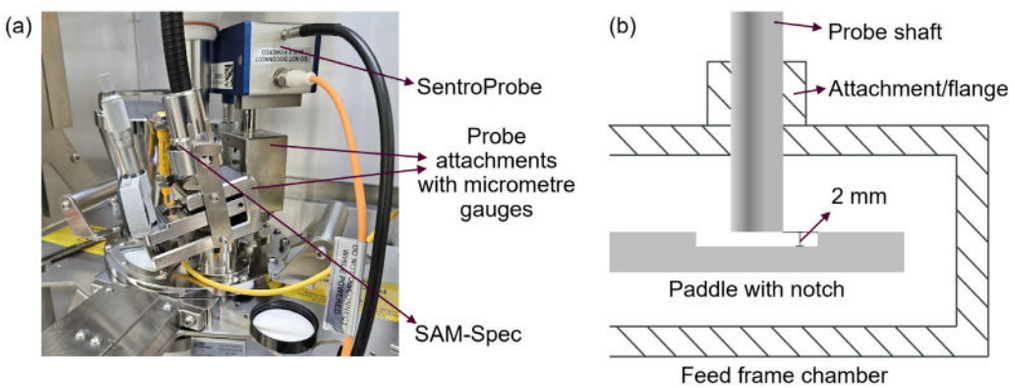


Fig. 3. (a) Probes inserted in the two PAT ports of the FFSIM with the (b) distance from the paddles at which they were positioned.

depth. The SAM-Spec probe has a diameter of 8.5 mm and was inserted into a sheath, which was then anchored to the adapter at an angle of 12° from the perpendicular to the chamber. It also had a micrometer gauge to adjust its depth into the chamber, as shown in Fig. 3(a). The integration time utilised, or the amount of time the spectrometer collects reflected light from the sample, was optimised with the signal intensity of the reference standard for each spectrometer. For the SentroPAT FO this corresponds to a value of approximately 40,000 to 50,000 counts when measuring the white reference standard, whereas for the Hy-Ternity it corresponds to approximately 90% intensity while measuring its respective white reference. The resulting integration times were 14 ms for the SentroPAT FO and 0.5 ms for the Hy-Ternity system.

2.3.3. Sample size determination

FDA guidance for the development and submission of NIR analytical procedures outlines that to obtain a representative sample size for in-line process monitoring, each NIR spectrum acquired should correspond to a unit dose of powder mass (FDA, 2021). However, accurately determining the sample size is complex, as work by Peeters et al. (2023) points out limitations including changes in the penetration depth of the light signal with wavelength, powder density, particle size and process parameters. Given the wide range of empirical and simulated values quoted in the literature between 0.28 mm and 0.7 mm, the NIR signal penetration depth is assumed to be 0.5 mm as that is the most commonly utilised estimation (Clarke et al., 2002; Peeters et al., 2023; Li et al., 2018, 2019; Rangel-Gil et al., 2024; Colón et al., 2014; Wahl et al., 2014; Shi and Anderson, 2010). For the NIR-SRS system, the estimated penetration depth utilised was increased to 1.5 mm to account for the longer path length the light takes prior to reaching the fibres further away from the illumination strip (Román-Ospino et al., 2021; Scheibelhofer et al., 2018).

To calculate the effective sample size, the settings of the spectrometer, geometry of the system used and powder properties must be taken into consideration. These can be used to estimate the powder sampled by one spectrometer measurement, or vice versa to calculate the required number of spectral averages to set in the respective instrument to achieve unit dose equivalence with each measurement. The method is based on the work by Li et al. (2019), which sums the volume of the moving powder captured at a specific angular velocity to the two half hemi-ellipsoids captured at the beginning and end of the acquisition. The sample size m was thus calculated using Eq. (1). It is determined by the powder density ρ, the radius of the probe spot ($r = 2.5$ mm for the SentroPAT FO and $r = 2.7$ mm for the Hy-Ternity), the signal penetration depth h, the time t required to collect one spectrum (given by the product of integration time and the number of spectral averages), the distance ($l = 65.7$ mm) between the centre of the paddle wheel and the centre of the probe spot and the angular velocity of the powder ($\omega = 0.5\ rps$), which is assumed to be equivalent to the paddle speed of the FFSIM.

$$m = \rho\pi rh\left(\omega tl\pi + \frac{2}{3}r\right) \tag{1}$$

Given the unit dose target was 100 mg for each tablet, the number of averages required to achieve this was calculated by rearranging Eq. (1) and varied for each instrument. The density was taken as the average of all the formulations as there were minimal changes between blends with different target compound loadings. All formulation densities deviated by up to a maximum of 0.05 g cm^{-3} from the mean values used, which were 0.41 g cm^{-3} for the lactose blends and 0.42 g cm^{-3} for Product A blends. As a result, the number of averages utilised for

PEMBROKE INSTRUMENTS
pembrokeinstruments.com | sales@pembrokeinstruments.com | +1-650-550-8618

PEMBROKE INSTRUMENTS, LLC
pembrokeinstruments.com | sales@pembrokeinstruments.com | +1-650-550-8618

the SentroPAT FO were 42 and 41 for lactose and Product A blends respectively, whereas for the Hy-Ternity system the averages used were 337 and 328 for lactose and Product A formulations respectively.

Once these were calculated, the measurement frequency was then evaluated. The number of averages (N) obtained and the integration time (I) utilised along with the processing time ($P = 0.107\ s$ for the SentroPAT FO and $P = 0.0017\ s$ for the Hy-Ternity, on average) of each instrument were used to determine the time taken for one measurement (t_m), according to Eq. (2).

$$t_m = I * N + P \tag{2}$$

Measurement time was maintained below 1 s to provide a sufficient data collection frequency for real-time assessment of blend quality, consistent with method deployment on a commercial tablet press. Both instruments met this constraint across lactose and Product A runs.

2.4. Model development

The raw data collected was analysed chemometrically using SIMCA® version 17.0 (Sartorius, Umeå, Sweden) to pre-process data and build the PCA static models for the stability tests as well as all dynamic models with the PLS regression algorithm. PLS was selected as it can robustly handle highly correlated spectral variables, extracting Latent Variables (LVs) that maximise covariance between spectral variance and API concentration for accurate quantification (Colaço Botelho Mestre, 2023). It reduces noise by focusing on chemically relevant variance and is widely validated for NIR quantitation.

2.4.1. Data pre-processing

Firstly, API peak identification was performed to determine the spectral regions of interest for lactose and Product A, which can be used to build more component specific models focusing on a narrower wavelength region and compare them with full spectrum models. Any noise at the edges of the spectra was similarly excluded, typically occurring in the initial portion of the spectrum close to the lower wavelengths. The data was then mean centred and various combinations of pre-processing were tested. Different smoothing techniques were explored, including 1st and 2nd derivatives, Savitzky–Golay and Asymmetric Least Squares (AsLS). Normalisation was applied via either Standard Normal Variate (SNV) or Peak Area Normalisation (PAN) surrounding the peak region of interest, in a range of combinations with the smoothing methods. These were applied to address different sources of unwanted spectral variation. The first derivative was used to reduce baseline offsets and enhance changes in spectral slope, whereas the second derivative was used to further minimise baseline effects and improve the resolution of overlapping bands. However, this increased sensitivity to noise. Savitzky–Golay preprocessing was used to smooth high-frequency noise while preserving spectral shape and, where applicable, to support derivative calculation with less noise amplification. Asymmetric least squares was applied for baseline correction to remove slowly varying background contributions. Regarding normalisation methods, SNV was used to reduce multiplicative scatter and path length related intensity differences, whereas peak area normalisation was used to reduce variability in overall spectral intensity and place spectra on a more comparable scale. These preprocessing steps were tested in combination since smoothing, derivative, or baseline-correction methods help reduce noise, drift, and band overlap, while subsequent normalisation reduces scatter-related and intensity-related variability. This sequential approach improved the emphasis on chemically relevant information within the spectra.

2.4.2. PLS regression and model performance evaluation

A range of resulting PLS models was obtained, with the number of LVs selected based on the balance between decreasing the Root Mean Square Error of Cross Validation (RMSECV) while maximising Q^2 and prioritising model simplicity (Román-Ospino et al., 2021). Q^2 is the cross-validated predictive squared correlation, which quantifies the predictive performance of a model, with values closer to 1 indicating strong agreement between predicted and observed concentration values. Each of the models includes 10 data points per concentration, for each of the 3 repeat blends. There was a randomised split of 70/30 between calibration and validation data points consistent with common chemometric practice and guidance for independent validation in spectroscopy, where 70% of the data were used in calibration models and the remaining 30% in validation models. This was selected to provide a sufficient balance of data for stable PLS calibration with an independent validation set large enough to provide an unbiased estimate of predictive performance. Although this split provided separate calibration and validation sets, both were derived from data collected under the same experimental conditions. As such, the validation primarily reflects internal model consistency and may overestimate generalisability to independently prepared blends, different material batches or altered process conditions. The models were evaluated by comparing Root Mean Squared Errors (RMSE), including of estimation (RMSEE) and of cross-validation (RMSECV) for calibration and of prediction (RMSEP) for validation models. These errors are standard for PLS as they collectively quantify model fit and generalisation, with RMSEE capturing the calibration fit, RMSECV assessing robustness via cross-validation, and RMSEP providing an unbiased estimate of predictive performance. To aid model interpretation, Variable Importance in Projection (VIP) plots were overlaid with the pre-processed spectrum of the pure target material. This enabled confirmation that the models were assigning greater importance to variables associated with spectral peaks of the compound being quantified. VIP scores were used to assess variable contributions to the predictive performance of the model, with values greater than 1 considered significant.

The Limit of Detection (LOD) and Limit of Quantitation (LOQ) were also calculated from the models, to quote the respective values for each formulation with each instrument specifically. They define the practical sensitivity limits of a quantitative model, where LOD marks the lowest concentration that can be reliably detected above noise, and LOQ marks the lowest concentration that can be quantified with acceptable precision, establishing the usable lower bound for calibration and routine monitoring. These were evaluated by utilising two variations of the International Council for Harmonisation (ICH) methodology, as outlined in the Validation of Analytical Procedures Q2 guidance (International Council for Harmonisation, 2023). The prediction error from the PLS model is used to represent noise and is multiplied by a numerical factor to determine LOD and LOQ (RMSEP method):

$$LOD = 3.3 \times RMSEP \tag{3}$$

$$LOQ = 10 \times RMSEP \tag{4}$$

or alternatively, the PLS model is used to estimate the two limits by focusing on the spread of values at low concentration as well as their overall trend in the model (standard deviation method).

$$LOD = \frac{3.3 \times \sigma}{S} \tag{5}$$

$$LOQ = \frac{10 \times \sigma}{S} \tag{6}$$

where σ is the standard deviation of the predictions at the lowest concentration and S is the slope of the PLS model curve (International Council for Harmonisation, 2023).

PEMBROKE INSTRUMENTS
pembrokeinstruments.com | sales@pembrokeinstruments.com | +1-650-550-8618

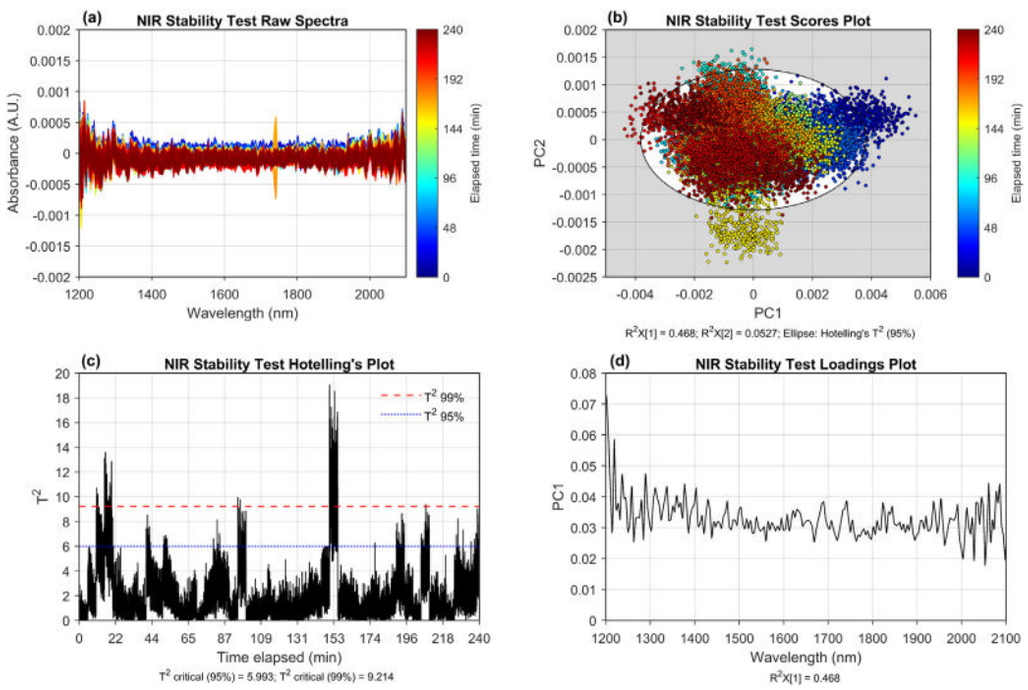


Fig. 4. PCA model for the Sentronic SentroPAT FO 4 h stability test: (a) raw spectra over time, (b) scores plot depicting how the spectra varied over time compared to the model space, (c) Hotelling's T^2 plot to show variability over time and (d) loadings plot for PC1.

3. Results and discussion

3.1. Signal stability of the Sentronic SentroPAT FO

The SentroPAT FO showed consistent stability throughout the 4 h long data collection of the white reference, with absorbance values fluctuating around the 0 A.U. reference value. The lower region of the spectrum between 1100 and 1200 nm has been excluded as it contains instrument noise. A temporary 10 min increase in the absolute value of the absorbance (both positively and negatively) was observed approximately 165 min after the start of the experiment, involving the wavelength region between 1733 nm and 1746 nm (Fig. 4(a)). The scores plot in Fig. 4(b) summarises the data described by PC1 and PC2 as fitting well within the model space, with a randomised distribution over time and the absence of a notable drift. A significant portion of the data collected in the initial 20 min lies outside the model space (95% confidence limit), as well as a cluster between 150 and 155 min. The Hotelling's T^2 plot shows the cyclical nature of the variability, with a drift correction every 5 min resetting the baseline reference values for the unit. Values mostly remained below the confidence limit critical lines outlined in red and blue, however there were some short instances where the data was drifting away from the model space and beyond those limits, as shown in Fig. 4(c). The most evident example is again between 150 and 155 min, where the values are consistently above the critical lines. There are no specific spectral regions driving the variability outlined in the model, as the contribution of each wavelength in the loadings plot remains near a steady baseline, with no pronounced peaks or distinct features (Fig. 4(d)).

Overall, the extremes of the spectrum present a higher level of noise as they are closer to the detection limits of the instrument, however the data is stable over time despite temporary increases in variability. A 1st derivative filter followed by SNV were applied for data pre-processing, with the aim to smooth the regions of variability in the Hotelling's T^2 plot (Fig. 5).

The PCA model performance improved by pre-processing, as most of the data can be described within the 95% confidence limits of the scores plot, except the intervals between 85 and 90 min as well as between 150 and 155 min, as shown in Fig. 5(a). Similarly, in the Hotelling's T^2 plot these are the only regions with data points above both the 95% and 99% confidence limit lines (Fig. 5(b)). The dataset is broadly uniform, however the drift correction at regular intervals induces a substantial baseline shift, at times pushing observations beyond the modelled space. Extending the interval may improve stability, yet it increases the risk of cumulative drift and potentially larger baseline adjustments at each scheduled correction.

3.2. Signal stability of the Indatech Hy-Ternity

The raw spectra showed a good level of agreement over time, with only minor differences in limited wavelength regions of the spectrum, such as around 1500 nm (Fig. 6(a)). The scores and Hotelling's T^2 plots show a 35 min region of drift occurring approximately 2 h after the experiment started (Fig. 6(b) and (c)). A significant drift over time is also reflected in the Hotelling's T^2 plot for the first 50 min approximately, with a continuous decrease in variability. The remaining observations over time fit into a stable baseline. The loadings plot does not indicate any particular wavelengths where the majority of the variability arises, since there are alternating spectral regions of higher and lower variability with PC 1, as shown in Fig. 6(d).

Pre-processing in the form of AsLS followed by SNV was then applied to smooth these regions of variability, but this was not fully achieved as the drift was still present (Fig. 7(a) and (b)). All the data points however fit beneath the standard deviation critical lines (dotted in red and blue) following pre-processing, highlighting the low overall variability.

The variability in the initial part of the test could be due to the warming up of the probe over time as the experiment progressed (despite starting the run after the warm-up period of the instrument), or the warming up of the sample itself. However, the latter is less likely since the white standard utilised does not thermally degrade and its signal should remain unaltered with minor temperature changes. It is also possible that this measured variation is insignificant in the context of measuring a dynamic powder sample, as this test simply

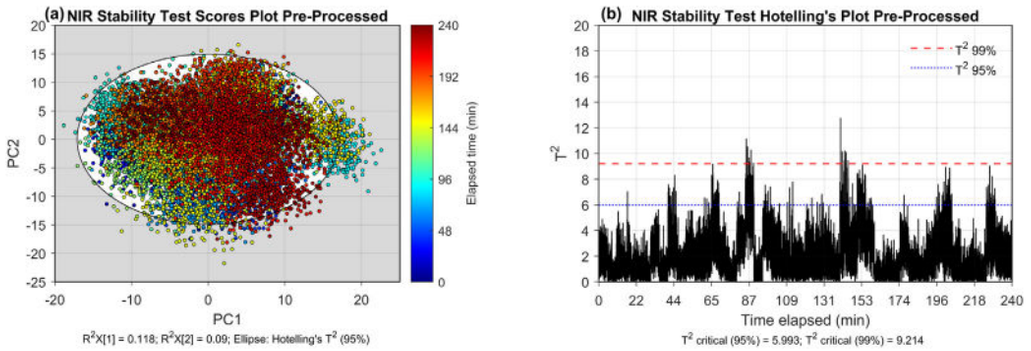


Fig. 5. SentroPAT FO stability test PCA model with 1st derivative and SNV pre-processed data showing the (a) scores and (b) Hotelling's T^2 plots.

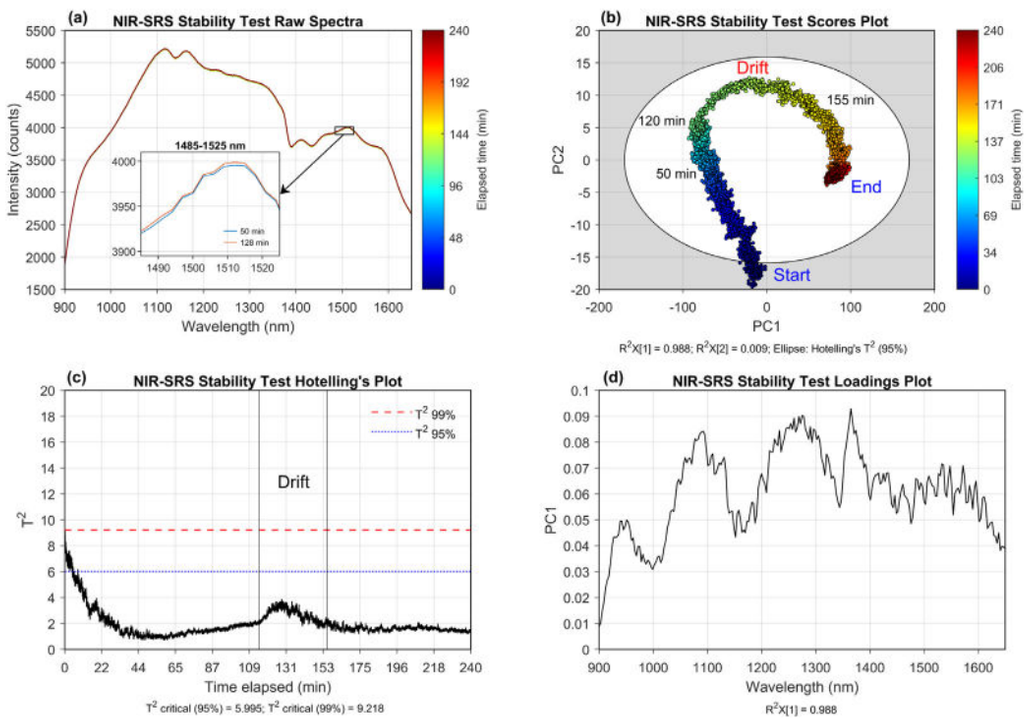


Fig. 6. PCA model for the Indatech Hy-Ternity 4 h stability test: (a) raw spectra over time with an inset showing a zoomed region around 1500 nm, (b) scores plot depicting how the spectra drifted over time compared to the model space, (c) Hotelling's T^2 plot to show variability over time and (d) loadings plot for PC1, highlighting differences in variability from specific regions in the spectrum.

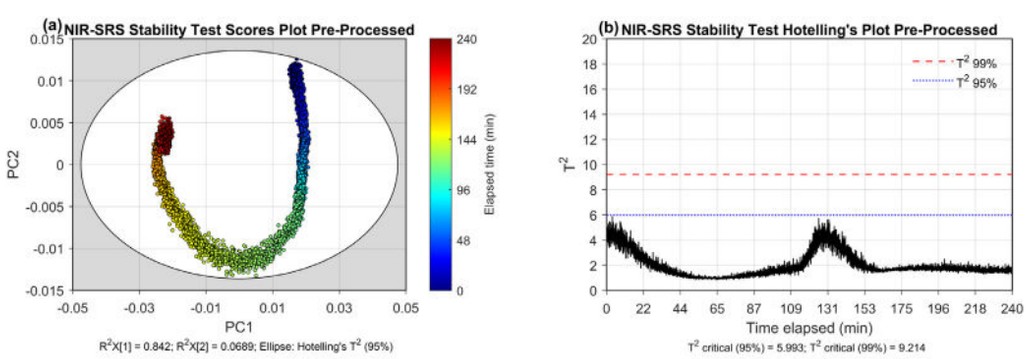


Fig. 7. Hy-Ternity stability test PCA model with 1st derivative and SNV pre-processed data showing the (a) scores and (b) Hotelling's T^2 plots.

examined the same static sample, emphasising any minor fluctuation in an otherwise stable measurement.

All the fibres presented marginally different features within the respective spectra, some with more pronounced peaks than others but

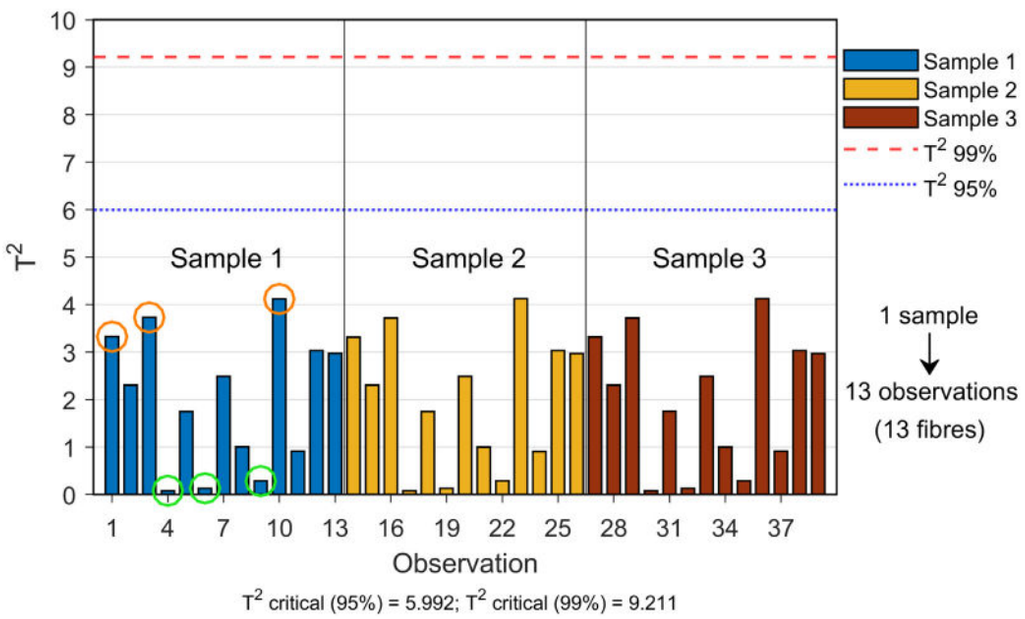


Fig. 8. Hotelling's T^2 bar chart for three measurements showing the variability between the different fibres. The most variable fibres are highlighted in orange circles (1, 3 and 10), while the least variable ones are circled in green (4, 6 and 9).

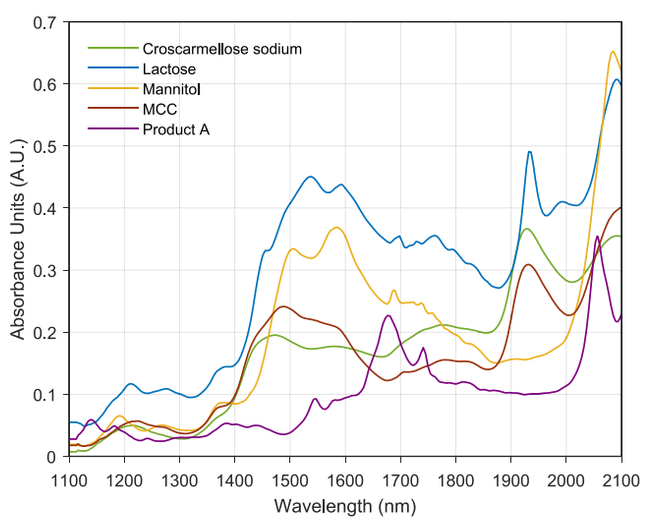


Fig. 9. Spectra of the pure components captured with the SentroPAT FO instrument.

all were consistent over time. A Hotelling's T^2 plot was used to identify that the fibres with the most variability as labelled in Fig. 2(b) were 1, 3 and 10, while the ones with the least variability were 4, 6 and 9 (Fig. 8).

As reported by Igne et al. (2015), the fibres closest to the illumination strip exhibit strong scattering phenomena, resulting in fewer spectral features and more variability, due to their proximity to the light source and thus greater signal interference. They tend to capture almost directly emitted light, as opposed to the fibres further away from the light source, which have higher absorbance due to the light travelling further through the sample (De Man et al., 2023).

3.3. Peak identification of pure components and wavelength selection

The characteristic peaks of the materials of interest were identified by plotting the spectra of all the pure components, as shown in Fig. 9.

Lactose peaks can be observed at 1932 nm, 2090 nm, 1537 nm and 1592 nm. Hence for the excipient formulations, reduced wavelength models of 1500–2000 nm for the SentroPAT FO NIR and 1400–1650 nm for the Hy-Ternity NIR-SRS have been tested to minimise the overlap with MCC peaks while maintaining a wide enough region to not compromise the model's ability to predict reproducibly. These regions can be used for wavelength selection and the performance of the resulting models is compared to those utilising the full spectrum. The spectral range for the NIR-SRS is significantly limited as half of the characteristic peaks outlined are located beyond the working range of the instrument, which reaches up to 1650 nm. Models focusing on a narrower wavelength range of 1550–2000 nm for NIR and 1500–1650 nm for NIR-SRS were also built to focus on the region of interest for Product A. However, the reduced wavelength range models for the excipient blends did not perform as well as the full range models after noise reduction, thus the wavelength ranges utilised were 1150–2100 nm for the NIR and 900–1650 nm for the NIR-SRS. For the Product A formulations, the reduced range model performed better only for the NIR instrument thus it was selected, whereas the full range was utilised for the NIR-SRS system. Removing large sections of the spectrum to focus on the regions with API peaks mostly reduced model capability of distinguishing different drug loadings, leading to worse performances (see Supporting Information Tables S1 and S2).

3.4. Spectral pre-processing and PLS models

The number of LVs was selected by plotting the value of Q^2 and RMSECV respectively against the number of components (see Supporting Information Figures S1–S4). When a plateau in both metrics was reached, the corresponding number of LVs was selected. For this application, 3 LVs were selected as they maximised Q^2 before reaching a plateau with minimal gains after addition of further LVs. Similarly, the RMSECV reached a minimum plateau around the same value. This achieved a parsimonious balance, minimising model complexity while maintaining a high performance. Various pre-processing combinations were tested and compared in terms of performance based on the root mean square errors of the resulting models. The pre-processing resulting in the lowest errors for the lactose models using NIR was SNV only, while for NIR-SRS it was AsLS correction with 100,000 smoothing and 0.001 symmetry followed by SNV. For Product A formulations

Table 2
Summary of API quantification model parameters for the two instruments with excipient and Product A formulations.

Instrument	Pre-processing selected	Calibration/Validation spectra (quantity)	Spectral range (nm)	LVs	RMSEE	RMSECV	RMSEP
Excipient formulations							
SentroPAT FO NIR	SNV	126/54	1150–2100	3	0.278	0.293	0.255
Hy-Ternity NIR-SRS	AsLS and SNV	126/54	900–1650	3	0.279	0.293	0.273
Product A formulations							
SentroPAT FO NIR	1st derivative	126/54	1550–2000	3	0.556	0.582	0.634
Hy-Ternity NIR-SRS	SNV and 1st derivative	126/54	900–1650	3	0.575	0.576	0.531

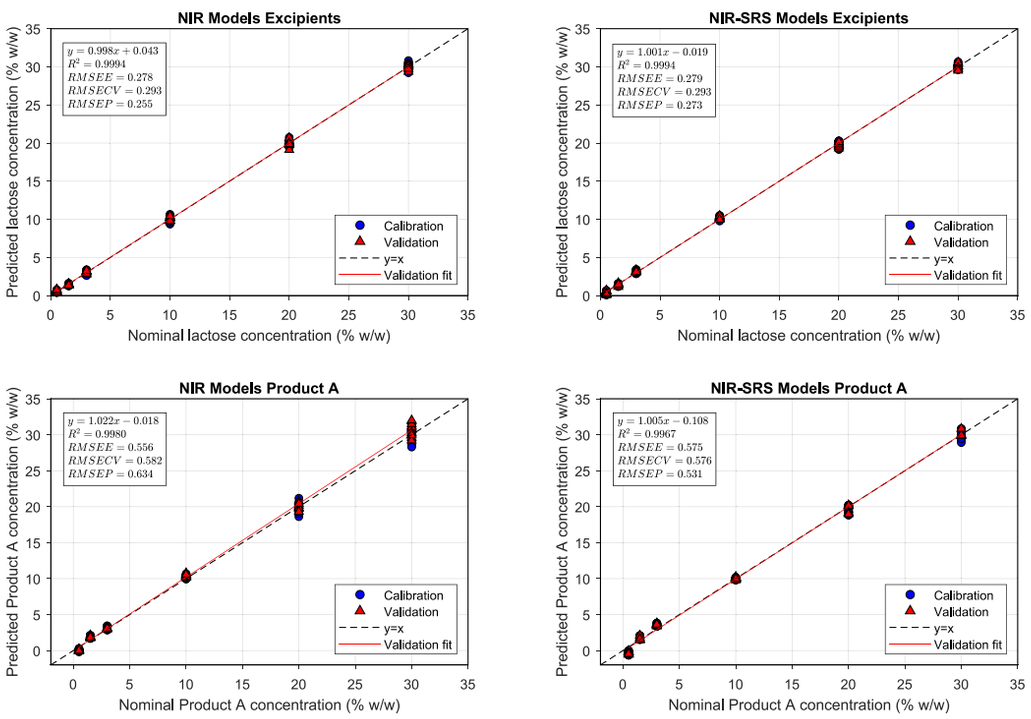


Fig. 10. PLS models of predicted against nominal target compound concentration for the SentroPAT FO NIR and the Hy-Ternity NIR-SRS instruments with both excipient and Product A formulations.

instead, it was 1st derivative with the NIR system, whereas it was SNV followed by 1st derivative with a 5 point window for the NIR-SRS instrument (Table 2, and see Supporting Information Tables S1 and S2). Comparison of the VIP plots with the spectra of the pure target compounds showed that multiple regions with VIP scores greater than 1 coincided with characteristic spectral bands of lactose and Product A, supporting the interpretation that the PLS models were driven by concentration related spectral variation (see Supporting Information Figure S5).

The resulting models for the two instruments and per formulation are shown in Fig. 10, including calibration and validation datasets.

Table 2 and the plots in Fig. 10 indicate a comparable performance of the two systems, which have very close RMSEs and highlight the very reproducible prediction capability of both instruments. This is in part due to the use of a validation set which was a randomised subset of the calibration data, therefore very similar to it and resulting in a good fit within in the model. However, as the same procedure was applied to both instruments for comparison purposes, it can still reflect the relative differences in predictive ability of the two units. The higher errors in the Product A models, especially at lower concentrations, can be attributed to inaccuracies during blend preparation rather than a modelling feature, as both instruments show a very similar behaviour where 0.5% w/w is under-predicted and 3% w/w is over-predicted. This does not imply an absence of heterogeneity, but rather suggests that, within the effective sampling scale of the measurements used, any such heterogeneity was similarly represented in both datasets. The main sources of inaccuracy include small weighing errors, minor material retention on the blender walls and limited material loss during powder transfer between containers or splitting between repeat experiments. This effect is also not present in the lactose models. This comparable performance was observed despite technological differences, with the NIR-SRS spectrometer collecting data from 13 fibres and averaging them, as opposed to a single collection fibre in the NIR instrument. In addition, the SentroPAT FO records absorbance values at every wavelength, whereas the Hy-Ternity system only records one data point every 3 wavelength numbers, reducing spectral granularity. The NIR-SRS unit also spans a narrower wavelength range of 750 nm rather than the 1000 nm of the NIR spectrometer, which can hinder model performance.

3.4.1. Narrower concentration models

To improve performance over narrower concentration ranges rather than looking at a wide spread of loadings, the Product A models were split into two more representative ranges: a low concentration one between 0.5% w/w and 3% w/w and another between 10% w/w and 30% w/w. These led to improved performances for both instruments as the models were closer to their respective target concentrations (Table 3). For the SentroPAT FO at both high and low concentrations models worked best utilising a reduced wavelength range around the API peaks of 1500–2000 nm. The Hy-Ternity system models for both high and low

PEMBROKE INSTRUMENTS, LLC
pembrokeinstruments.com | sales@pembrokeinstruments.com | +1-650-550-8618

Table 3
Summary of API quantification model parameters for low and high concentrations models with the two instruments on Product A formulations. The RMSE values in brackets are normalised by the model concentration range.

Instrument	Pre-processing selected	Calibration/Validation spectra (quantity)	Spectral range (nm)	LVs	RMSEE	RMSECV	RMSEP
Low concentration Product A formulations (0.5% w/w to 3% w/w)							
SentroPAT FO NIR	2nd derivative	63/27	1550–2000	3	0.092 (3.68)	0.100 (4.00)	0.091 (3.64)
Hy-Ternity NIR-SRS	SNV and 1st derivative	63/27	900–1650	3	0.086 (3.44)	0.084 (3.36)	0.080 (3.20)
High concentration Product A formulations (10% w/w to 30% w/w)							
SentroPAT FO NIR	1st derivative and S-G	63/27	1550–2000	3	0.564 (2.82)	0.590 (2.95)	0.422 (2.11)
Hy-Ternity NIR-SRS	SNV and 1st derivative	63/27	900–1650	3	0.314 (1.57)	0.351 (1.76)	0.212 (1.06)

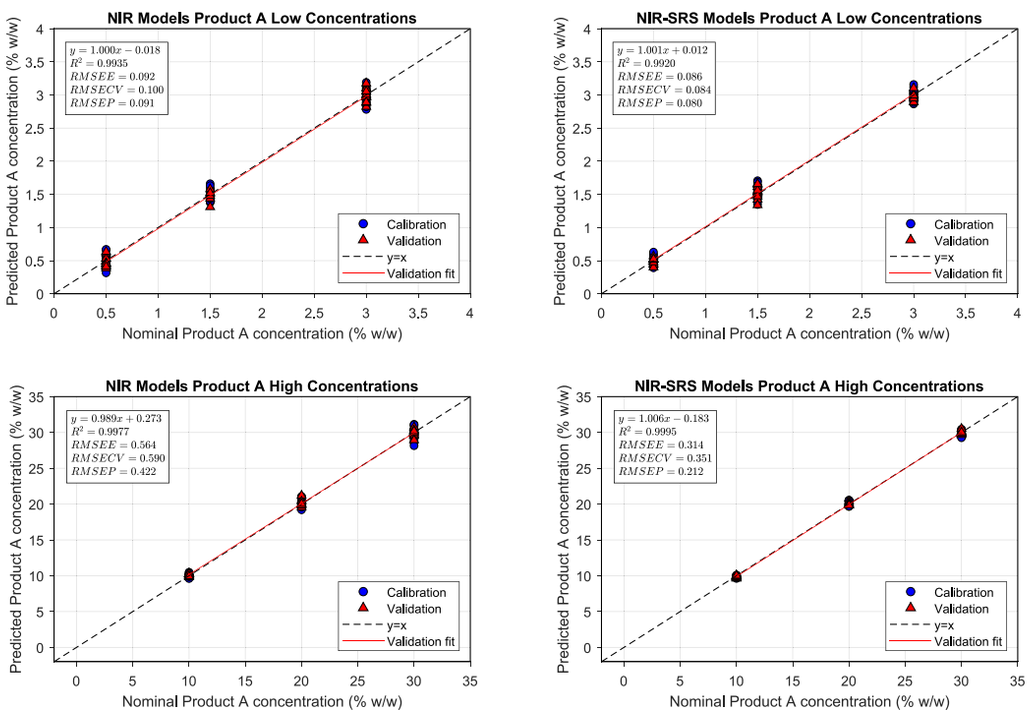


Fig. 11. PLS models of predicted against nominal target compound concentration for the SentroPAT FO NIR and the Hy-Ternity NIR-SRS instruments with Product A formulations at low and high concentrations.

concentrations worked best with the full wavelength range, as shown in Fig. 11. The RMSE values are also quoted as a percentage of the concentration range spanned by each model, making the low- and high-concentration models directly comparable. VIP plots for these models are provided in Supporting Information Figure S6.

The percentage RMSE values indicate that the two ranges perform similarly once the effect of modelling significantly different concentrations is removed, with the higher Product A loading models slightly outperforming the lower loading ones. The Hy-Ternity instrument consistently performed marginally better compared to the SentroPAT FO, for both low and high Product A concentrations. However, it is advisable to build models which have at least 5 concentration points to maximise reproducibility and make them more adaptable to unknown concentrations, thus avoiding overfitting.

3.4.2. NIR-SRS fibres data and models

To further increase model performance for NIR-SRS, only the data from the outermost external fibres, 10 to 13, was utilised to check if instrument performance and model predictive ability could be improved. As discussed in Section 3.2, external fibres allow light to travel further into the sample resulting in a longer path length and are thus the most suitable to build predictive models (Igne et al., 2015; Román-Ospino et al., 2021). This was achieved by taking both the average of these 4 fibres as well as considering all the data from the individual fibres into the model. A similar test was done by utilising data from the most stable fibres as shown in Fig. 8, thus fibres 4, 6 and 9, which were also averaged and taken individually in separate models. The results are shown in Table 4 and Fig. 12, with VIP plots for the models reported in Supporting Information Figure S7.

Selecting and grouping some of the most stable fibres together to compare their performance with the mean data models did not bring significant advantages, as the resulting RMSEs are comparable. Consistent with Igne et al. (2015), NIR-SRS captures the same information as single point measurement NIR at the same spatial scale. However, they also observed that outermost fibres, farther from the illumination source, exhibited higher absorbance than central fibres. Following that rationale, Román-Ospino et al. (2021) prioritised using the outer fibres to enhance model performance from the collected data, which was also adopted and tested in the present study. Utilising the data from each of the selected fibres individually caused a decrease in model performance, with higher error values compared to the averaged fibres data. Therefore even with fibre selection, the performance of the two instruments can be considered very similar, with only marginally lower errors for the Hy-Ternity system compared to the SentroPAT FO.

PEMBROKE INSTRUMENTS
pembrokeinstruments.com | sales@pembrokeinstruments.com | +1-650-550-8618

Table 4
Summary of API quantification model parameters for NIR-SRS fibre data on Product A formulations.

Instrument	Pre-processing selected	Calibration/Validation spectra (quantity)	Spectral range (nm)	LVs	RMSEE	RMSECV	RMSEP
External fibres (F 10–13)							
Hy-Ternity NIR-SRS individual fibres	2nd derivative and SNV	504/216	900–1650	3	0.821	0.858	0.834
Hy-Ternity NIR-SRS averaged fibres	SNV and 1st derivative	126/54	900–1650	3	0.548	0.547	0.603
Most stable fibres (F 4, 6 and 9)							
Hy-Ternity NIR-SRS individual fibres	1st derivative and Peak Area Normalisation	378/162	900–1650	3	0.933	0.947	0.944
Hy-Ternity NIR-SRS averaged fibres	SNV and 1st derivative	126/54	900–1650	3	0.551	0.555	0.652

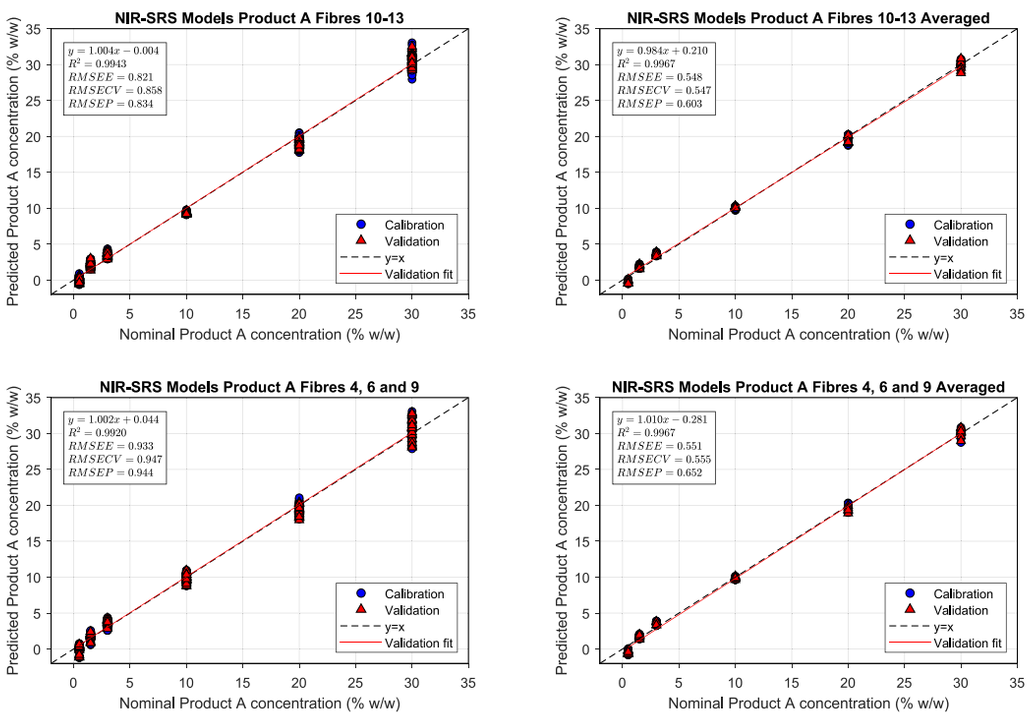


Fig. 12. PLS models of predicted against nominal target compound concentration for the Hy-Ternity NIR-SRS instrument with Product A formulations utilising selected fibres both individually and averaged.

Table 5
Estimated LOD and LOQ values for both instruments with excipient and Product A formulations.

Instrument	RMSEP LOD (% w/w)	RMSEP LOQ (% w/w)	σ LOD (% w/w)	σ LOQ (% w/w)
Excipient formulations				
SentroPAT FO NIR	0.841	2.548	0.442	1.339
Hy-Ternity NIR-SRS	0.901	2.729	0.724	2.195
Product A formulations				
SentroPAT FO NIR	2.091	6.335	0.271	0.821
Hy-Ternity NIR-SRS	1.751	5.307	0.563	1.705

3.5. LOD and LOQ evaluation

As an additional comparison, performance can be quantitatively evaluated by looking at the LOD and LOQ of the two instruments with the same conditions and formulations. The results are shown in Table 5.

The LOD and LOQ values reinforce the previous results of a comparable performance between the two instruments, which are both able to detect lower concentrations of lactose compared to Product A in the blend. This could be due to the lack of spectral features in Product A compared to lactose, causing it to be more complex to distinguish chemometrically amongst the excipients in the formulation. In addition, all the LOD values remain below 0.9% w/w for excipient and 2.1% w/w for Product A blends, indicating that the spectrometers are suitable for model building with a range of target compound concentrations in the blend down to those amounts as the minimum threshold. However, these performances show that the systems may not be sufficient for low dose formulations below 1% w/w. The limits of quantitation are higher, with a maximum of 2.7% w/w for excipient and 6.3% w/w for Product A formulations, thus models developed at or above these concentrations provide quantitatively reliable predictions without the need for further optimisation. Although the model data applied down to 0.5% w/w within the context of this study, confidence in performance at the lowest concentrations is limited and should not be interpreted as full validation of sub 1% w/w quantification capability, as reflected by the LOD and LOQ estimates. Further model development and independent validation would therefore be required to establish

PEMBROKE INSTRUMENTS, LLC
pembrokeinstruments.com | sales@pembrokeinstruments.com | +1-650-550-8618

the performance of either technique for robust routine quantification at such concentrations.

Overall, the RMSEP-based method is a chemometric adaptation of the ICH Q2 guidance and should be interpreted as an approximation, contingent on model linearity and representative validation. Despite the resulting values being in the expected range for such instruments, this method tends to over estimate the LOD and LOQ values compared to other methods. It considers all concentrations in the model and introduces overall fit errors away from the detection limit, whereas the standard deviation method is more focused around noise at the lower end of the concentration range, closer to the concentration limits themselves.

4. Conclusions

A side-by-side comparison was performed between single point measurement NIR spectroscopy (SentroPAT FO) and NIR-SRS (Hy-Ternity) using the feed frame simulator, enabling simultaneous PAT instrument evaluation on the same powder blends. The SentroPAT FO allows rapid data collection suitable for in-line applications via a single fibre, with high spectral resolution and a wide wavelength range. The Hy-Ternity system offers notable features including multiple collection fibres (13 were utilised in this study), a very fast integration time and a compact, easily installed probe with a user-friendly software.

Across the investigated formulations and operating conditions, the two spectrometers exhibited comparable performance, each accurately identifying and quantifying the target compound in dynamic powder flow with similar reproducibility. While NIR-SRS provides practical advantages, such as a high acquisition speed and spatial sampling across multiple fibres, these are significantly outweighed by its much narrower spectral range and reduced spectral resolution (one data point every three wavelength numbers). In this application, the NIR instrument provides almost twice the spectral coverage of NIR-SRS. Given that the specific key peaks for both lactose and Product A are mostly located above 1650 nm, these were unavailable to NIR-SRS for model building. The absence of this region and the lower spectral granularity limited NIR-SRS model performance and did not result in the expected increase in sensitivity that was hypothesised. Therefore in this application, the limited spectral coverage had a stronger influence on quantitative performance compared to the enhanced spatial resolution. This trade-off does not isolate these factors but rather reflects their combined effect within the commercially available probe configurations tested.

Despite these constraints, NIR-SRS delivered results comparable to NIR for the materials tested, including commercially relevant formulations, suggesting that expanding its accessible wavelength range and increasing resolution could enable it to match or exceed NIR performance for a range of products. This is particularly significant in low-dose contexts where broader spectral information improves model robustness and sensitivity (Bouckaert et al., 2025). Particle size was not independently characterised in this study and was not included as a specific experimental variable. Thus it may have contributed to non-linear effects in some of the models, particularly where the powder components differed significantly in particle size. However, as the aim of the work was to directly compare the two probes under identical measurement conditions, with both instruments acquiring data simultaneously from the same powder blends, any particle size-related variation was common to both techniques within the study design. Further studies could benefit from direct particle size characterisation to further assess its influence on spectral response and model performance. Similarly, paddle speed was kept constant throughout the study to isolate the comparison between the two spectroscopic techniques and avoid introducing an additional experimental variable. The conclusions are therefore limited to the selected controlled operating conditions. As such, the possible interaction of paddle speed with blend properties and its effects on spectral response or model performance were not investigated in this work and further investigation of these aspects would be valuable, particularly regarding robustness evaluations and process sensitivity.

Future investigations should explore additional powder systems featuring challenging target components to identify spectroscopically as well as low-dose APIs. Additionally, employing a NIR-SRS system with a broader spectral range and higher sampling granularity would enable a more direct comparison with single point measurement NIR. Such work would clarify the extent to which improved spectral coverage can enhance NIR-SRS performance and support robust real-time release testing models across a broader range of products. Comparisons with alternative PAT instruments can also be performed, including other types of spectroscopy, to benchmark sensitivity and specificity for low-dose formulations and assess complementary spectral information. Cross-spectroscopy studies could further evaluate robustness under dynamic feed frame conditions, enabling an informed selection or hybrid deployment of PAT sensors in continuous tableting.

CRediT authorship contribution statement

Eleonora De Giorgi: Writing – review & editing, Writing – original draft, Visualization, Methodology, Investigation, Formal analysis, Data curation. **Sean Clifford:** Supervision, Resources, Project administration, Funding acquisition, Conceptualization. **Kevin Sutcliffe:** Writing – review & editing, Supervision, Resources, Project administration, Funding acquisition, Conceptualization. **Nathan Cumberbatch:** Writing – review & editing, Supervision, Resources, Project administration, Funding acquisition, Conceptualization. **Estefania Lopez-Quiroga:** Writing – review & editing, Supervision, Resources, Project administration. **Christopher Windows-Yule:** Writing – review & editing, Supervision, Resources, Project administration, Conceptualization.

Declaration of competing interest

The authors declare the following financial interests/personal relationships which may be considered as potential competing interests: Eleonora De Giorgi reports financial support, administrative support, and equipment, drugs, or supplies were provided by AstraZeneca UK Limited. If there are other authors, they declare that they have no known competing financial interests or personal relationships that could have appeared to influence the work reported in this paper.

Acknowledgements

This work was sponsored by AstraZeneca UK Limited and the Centre for Doctoral Training (CDT) at The University of Birmingham, with funding from the Engineering and Physical Sciences Research Council (EPSRC) - grant number EP/L015153/1. Special thanks to Dr Andrew Ingram for providing invaluable insights and suggestions throughout the study, as well as Dr Matt Bunker and Dr Peter Hamilton for the supervision and support.

Appendix A. Supplementary data

Supplementary material related to this article can be found online at https://doi.org/10.1016/j.ijpharm.2026.127174.

Data availability

Data will be made available on request.

PEMBROKE INSTRUMENTS
pembrokeinstruments.com | sales@pembrokeinstruments.com | +1-650-550-8618

References

Bhimrao, L.S., Kumar, S., Agrawal, A.K., Beer, T.D., Kumar, A., Kumar, D., 2026. Continuous manufacturing in pharmaceuticals: an integrated approach with NIR and Raman as PAT tools. http://dx.doi.org/10.1016/j.ijpharm.2025.126478.

Bouckaert, L., De Man, A., De Souter, L., Starsich, F., Meir, B., Sowinski, S., Vervaet, C., De Beer, T., Vanhoorne, V., 2025. In-line NIR spectroscopy for comprehensive process understanding of semi-continuous blending in continuous production of low-dose formulations. Int. J. Pharm. 681, http://dx.doi.org/10.1016/j.ijpharm.2025.125622.

Brouckaert, D., Vandenbroucke, F., Chauchard, F., Dollinger, M., Roggo, Y., Pellegatti, L., Krumme, M., 2022. Towards real-time release of pharmaceutical tablets: 100% in-line control via near-infrared spatially resolved spectroscopy and 3D microwave resonance technology. J. Pharm. Biomed. Anal. 209, http://dx.doi.org/10.1016/j.jpba.2021.114491.

Clarke, F.C., Hammond, S.V., Jee, R.D., Offat, A.C.M., 2002. Determination of the Information Depth and Sample Size for the Analysis of Pharmaceutical Materials Using Reflectance Near-Infrared Microscopy. Technical Report 11, Vol. 56, p. 1475.

Colaço Botelho Mestre, H.A., 2023. Ensuring Blend Uniformity Inside the Feed Frame Simulator in the Development of PAT Models. Technical Report.

Colón, Y.M., Florian, M.A., Acevedo, D., Méndez, R., Romañach, R.J., 2014. Near infrared method development for a continuous manufacturing blending process. J. Pharm. Innov. 9 (4), 291–301. http://dx.doi.org/10.1007/s12247-014-9194-1.

De Leersnyder, F., Peeters, E., Djalabi, H., Vanhoorne, V., Van Snick, B., Hong, K., Hammond, S., Liu, A.Y., Ziemons, E., Vervaet, C., De Beer, T., 2018. Development and validation of an in-line NIR spectroscopic method for continuous blend potency determination in the feed frame of a tablet press. J. Pharm. Biomed. Anal. 151, 274–283. http://dx.doi.org/10.1016/j.jpba.2018.01.032.

De Leersnyder, F., Vanhoorne, V., Kumar, A., Vervaet, C., De Beer, T., 2019. Evaluation of an in-line NIR spectroscopic method for the determination of the residence time in a tablet press. Int. J. Pharm. 565, 358–366. http://dx.doi.org/10.1016/j.ijpharm.2019.05.006.

De Man, A., Uyttersprot, J.S., Chavez, P.F., Vandenbroucke, F., Bovart, F., De Beer, T., 2023. The application of near-infrared spatially resolved spectroscopy in scope of achieving continuous real-time quality monitoring and control of tablets with challenging dimensions. Int. J. Pharm. 641, http://dx.doi.org/10.1016/j.ijpharm.2023.123064.

Expo Process Analytics, FFSim™ Data Sheet. Technical Report. URL: www.expoprocessanalytics.com.

FDA, 2004. Guidance for Industry PAT - A Framework for Innovative Pharmaceutical Development, Manufacturing, and Quality Assurance. Technical Report, URL: http://www.fda.gov/cvm/guidance/published.html.

FDA, 2018. Bioanalytical Method Validation Guidance for Industry Biopharmaceutics Bioanalytical Method Validation Guidance for Industry Biopharmaceutics Contains Nonbinding Recommendations. Technical Report, URL: http://www.fda.gov/Drugs/GuidanceComplianceRegulatoryInformation/Guidances/default.htmand/orhttp://www.fda.gov/AnimalVeterinary/GuidanceComplianceEnforcement/GuidanceforIndustry/default.htm.

FDA, 2021. Development and Submission of Near Infrared Analytical Procedures Guidance for Industry. Technical Report, URL: https://www.fda.gov/drugs/guidance-compliance-regulatory-information/guidances-drugs.

Igne, B., Talwar, S., Feng, H., Drennen, J.K., Anderson, C.A., 2015. Near-infrared spatially resolved spectroscopy for tablet quality determination. J. Pharm. Sci. 104 (12), 4074–4081. http://dx.doi.org/10.1002/jps.24618.

International Council for Harmonisation, 2023. Validation of Analytical Procedures Q2(R2). Technical Report.

Li, Y., Anderson, C.A., Drennen, J.K., Airiau, C., Igne, B., 2018. Method development and validation of an inline process analytical technology method for blend monitoring in the tablet feed frame using Raman spectroscopy. Anal. Chem. 90 (14), 8436–8444. http://dx.doi.org/10.1021/acs.analchem.8b01009.

Li, Y., Anderson, C.A., Drennen, J.K., Airiau, C., Igne, B., 2019. Development of an in-line near-infrared method for blend content uniformity assessment in a tablet feed frame. Appl. Spectrosc. 73 (9), 1028–1040. http://dx.doi.org/10.1177/0003702819842189.

Ortega-Zúñiga, C.A., Román-Ospino, A.D., Gupta, S., Omar, T., Baranwal, Y., Sanchez-Paternina, A., Zhou, Q., Jing, J., Muzzio, F.J., 2025. Real-time monitoring of small changes in powder blends and ejected tablets in a low-dose formulation with 1 %w/w of active pharmaceutical ingredient using Raman and near-infrared spatially resolved spectroscopy within a tablet press. Int. J. Pharm. 670, http://dx.doi.org/10.1016/j.ijpharm.2025.125165.

Palmer, J., O'Malley, C.J., Wade, M.J., Martin, E.B., Page, T., Montague, G.A., 2020. Opportunities for process control and quality assurance using online NIR analysis to a continuous wet granulation tableting line. J. Pharm. Innov. 15 (1), 26–40. http://dx.doi.org/10.1007/s12247-018-9364-7.

Peeters, M., Peeters, E., Van Hauwermeiren, D., Cogoni, G., De Beer, T., 2023. Effect of process parameters and formulation properties on the lead-lag between in-line NIR tablet press feed frame and off-line NIR tablet measurements. Eur. J. Pharmaceut. Biopharmaceut. 189, 251–263. http://dx.doi.org/10.1016/j.ejpb.2023.06.012.

Rangel-Gil, R.S., Nasrala-Álvarez, J.M., Romañach, R.J., Méndez, R., 2024. Blend uniformity monitoring in a continuous manufacturing mixing process for a low-dosage formulation using a stream sampler and near infrared spectroscopy. Int. J. Pharm. 661, http://dx.doi.org/10.1016/j.ijpharm.2024.124478.

Román-Ospino, A.D., Baranwal, Y., Li, J., Vargas, J., Igne, B., Bate, S., Brouckaert, D., Chauchard, F., Hausner, D., Ramachandran, R., Singh, R., Muzzio, F.J., 2021. Sampling optimization for blend monitoring of a low dose formulation in a tablet press feed frame using spatially resolved near-infrared spectroscopy. Int. J. Pharm. 602, http://dx.doi.org/10.1016/j.ijpharm.2021.120594.

Rosas, J.G., Brush, P., Thompson, B., Miller, C., Overton, P., Tugby, N., Stoliarskaia, D., Hurley, S., Ramasamy, M., Conway, S.L., 2023. Implementation of a fully integrated CM direct compression and coating process at a commercial pharmaceutical facility – Part 2: PAT and RTD results for normal operational conditions batches. Int. J. Pharm. 636, http://dx.doi.org/10.1016/j.ijpharm.2023.122814.

Ryckaert, A., Cannon, M., Beer, T.D., Kumar, A., 2025. Tablet diversion strategy based on in-line NIR tablet press feed frame measurements. Int. J. Pharm. 670, http://dx.doi.org/10.1016/j.ijpharm.2025.125212.

Scheibelhofer, O., Wahl, P.R., Larchevêque, B., Chauchard, F., Khinast, J.G., 2018. Spatially resolved spectral powder analysis: Experiments and modeling. Appl. Spectrosc. 72 (4), 521–534. http://dx.doi.org/10.1177/0003702817749839.

Shi, Z., Anderson, C.A., 2010. Application of Monte Carlo simulation-based photon migration for enhanced understanding of near-infrared (NIR) diffuse reflectance. Part I: Depth of penetration in pharmaceutical materials. J. Pharm. Sci. 99 (5), 2399–2412. http://dx.doi.org/10.1002/jps.22013.

Sierra-Vega, N.O., Romañach, R.J., Méndez, R., 2019. Feed frame: The last processing step before the tablet compaction in pharmaceutical manufacturing. http://dx.doi.org/10.1016/j.ijpharm.2019.118728.

Wahl, P.R., Fruhmann, G., Sacher, S., Straka, G., Sowinski, S., Khinast, J.G., 2014. PAT for tableting: Inline monitoring of API and excipients via NIR spectroscopy. Eur. J. Pharmaceut. Biopharmaceut. 87 (2), 271–278. http://dx.doi.org/10.1016/j.ejpb.2014.03.021.